SCIENTIFIC REPORTS

SUBJECT AREAS:
TWO-DIMENSIONAL MATERIALS
SYNTHESIS AND PROCESSING
SOLID-PHASE SYNTHESIS
ELECTRICAL AND ELECTRONIC ENGINEERING

Received
5 April 2013

Accepted
7 May 2013

Published
21 May 2013

Correspondence and requests for materials should be addressed to L.C. (lcao2@ncsu.edu)

Controlled Scalable Synthesis of Uniform, High-Quality Monolayer and Few-layer MoS_2 Films

Yifei Yu[1], Chun Li[1], Yi Liu[3], Liqin Su[4], Yong Zhang[4] & Linyou Cao[1,2]

[1]Department of Materials Science and Engineering, North Carolina State University, Raleigh NC 27695, [2]Department of Physics, North Carolina State University, Raleigh NC 27695, [3]Analytical Instrumentation Facility, North Carolina State University, Raleigh NC 27695, [4]Department of Electrical and Computer Engineering, The University of North Carolina at Charlotte, Charlotte, NC 28223.

Two dimensional (2D) materials with a monolayer of atoms represent an ultimate control of material dimension in the vertical direction. Molybdenum sulfide (MoS_2) monolayers, with a direct bandgap of 1.8 eV, offer an unprecedented prospect of miniaturizing semiconductor science and technology down to a truly atomic scale. Recent studies have indeed demonstrated the promise of 2D MoS_2 in fields including field effect transistors, low power switches, optoelectronics, and spintronics. However, device development with 2D MoS_2 has been delayed by the lack of capabilities to produce large-area, uniform, and high-quality MoS_2 monolayers. Here we present a self-limiting approach that can grow high quality monolayer and few-layer MoS_2 films over an area of centimeters with unprecedented uniformity and controllability. This approach is compatible with the standard fabrication process in semiconductor industry. It paves the way for the development of practical devices with 2D MoS_2 and opens up new avenues for fundamental research.

The significance of 2D materials has been manifested by a plethora of fascinating functionality demonstrated in graphene, a monolayer material of carbon atoms[1–4]. In contrast to graphene, which is a semi-metal with no bandgap by nature, MoS_2 monolayers offer an attractive semiconductor option due to a direct bandgap of 1.8 eV[5,6]. This non-trivial bandgap makes MoS_2 monolayers a better candidate than graphene to revolutionize many electronic and photonic devices that are currently dominated by traditional group IV or III–V semiconductor materials[7–23]. Considerable efforts have been dedicated to achieve scalable synthesis of high quality MoS_2 monolayers that is necessary for the development of practical devices. These include sulfurization of MoO_3 or Mo layers pre-deposited on substrates, or thermolysis of Mo compound $(NH_4)_2MoS_4$[24–31]. However, none of the existing processes provides the capability to exclusively produce uniform MoS_2 monolayers over a large area up to centimeters. Additionally, none of these processes is able to precisely control the layer number of MoS_2 films. For instance, MoS_2 monolayers resulted from these processes always co-exist with by-products of thicker layers. As the properties of MoS_2 materials strongly depend on the layer number, this unsatisfactory uniformity and controllability poses a formidable challenge for the improvement of device performance. Here we present a new, self-limiting chemical vapor deposition (CVD) approach that can exclusively grow high-quality monolayer or few-layer MoS_2 films over an area of centimeters on various substrates such as silicon oxide, sapphire, and graphite. The layer number of the MoS_2 films can be precisely controlled as 1, 2, 3, and beyond. The synthesized film shows unprecedented uniformity with no other layers found by thorough characterizations. It exhibits optical and electrical quality comparable to the MoS_2 exfoliated from bulk materials, and can be transferred to other arbitrary substrates.

Results

We grew MoS_2 films at high temperatures ($> 800^\circ C$) using $MoCl_5$ and sulfur as precursor materials (we found the quality of resulting thin films worse at lower growth temperatures). The precursor materials can react at elevated temperatures to produce MoS_2 species, which may subsequently precipitate onto receiving substrates to yield MoS_2 films (Fig. S1). The layer number of the resulting MoS_2 films can be very precisely controlled by controlling the amount of $MoCl_5$ used in experiments or the total pressure in the synthetic setup (details see Studies of growth mechanism in the Supplementary Information). We have successfully grown monolayer or few-layer MoS_2 films on various substrates including silicon oxide, sapphire, and graphite. Fig. 1 a–b show optical images of the MoS_2

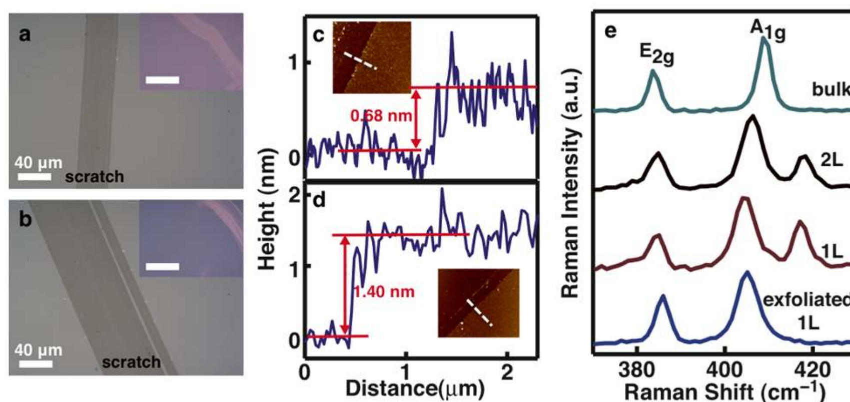

Figure 1 | Controlled synthesis of MoS_2 monolayer and bilayer films. (a) and (b), Optical images of the MoS_2 monolayer and bilayer films grown on sapphire substrates, respectively. The insets are optical images of the MoS_2 monolayer and bilayer films grown on SiO_2/Si substrates. The scale bars in the insets are 80 µm. (c) and (d), AFM height profiles for typical MoS_2 monolayer and bilayer films grown on sapphire, respectively. The insets show the AFM images from which the height profiles are extracted. A larger version of the AFM images is given in Fig.S3 of the Supplementary Information. (e), Raman spectra of the MoS_2 monolayer (1 L) and bilayer (2 L) films grown on sapphire. Also given are the Raman spectra of exfoliated MoS_2 monolayer and bulk MoS_2 dispersed on SiO_2/Si substrates. The two characteristic Raman modes are labeled. The peak at 418 cm^{-1} is from the sapphire substrate.

monolayer and bilayer films grown on sapphire substrates. The optical images of MoS_2 monolayer and bilayer films grown on silicon substrates with 280 nm thick silicon oxide (SiO_2/Si) are also given as insets. Scratches were intentionally introduced to show the color contrast between the thin film and the substrate (no MoS_2 film exists in the scratched area). We confirm the chemical composition of the thin films is MoS_2 using x-ray photoelectron spectroscopy (XPS) characterizations (Fig. S2). From the optical images, we can find that the thin films are continuous and uniform over a large area. We can also find that the color contrasts of MoS_2 monolayer and bilayer films bear little difference on sapphire but are substantially different on SiO_2/Si, the monolayer showing pink color while the bilayer more bluish. This substantial difference in color contrast may provide a facile approach to determine the thickness of 2D MoS_2 materials.

We characterized the synthesized thin films using atomic force microscope (AFM) and Raman spectroscopy. The thickness of the synthesized MoS_2 monolayers and bilayers are shown 0.68 nm and 1.40 nm (Fig. 1c–d), in consistence with exfoliated MoS_2 (Fig. S3–S5). Fig. 1e shows the Raman spectra collected from the as-grown MoS_2 thin films on sapphire with different layer numbers (the Raman spectra for the MoS_2 films grown on SiO_2/Si is given in Fig. S6). The Raman spectra of exfoliated MoS_2 monolayers and bulk MoS_2 materials are also given in Fig. 1e as references. Two characteristic Raman modes can be found in the spectra, the A_{1g} mode associated with the out-of-plane vibration of sulfur atoms and the E^1_{2g} mode related with the in-plane vibration of Mo and sulfur atoms[32–34]. The full width at half maximum (FWHM) of the E^1_{2g} peak may be used as an indicator for crystalline quality. The E^1_{2g} FWHM of the synthesized MoS_2 monolayer is 4.2 cm^{-1}, close to that of the exfoliated monolayer, 3.7 cm^{-1}. This suggests a good crystalline quality in the synthesized film. Additionally, the frequency difference (Δk) between the E^1_{2g} and A_{1g} modes has been known closely related with the layer number, and can be used to determine the thickness of MoS_2 materials[32–34]. We can find that the frequency difference Δk of the synthesized thin film increases with the thickness (Fig. 1e), consistent with what were observed on exfoliated MoS_2[32–34]. A systematic correlation between the value of Δk and the layer number of the synthesized film is given in Table S1 of the Supplementary Information. The Δk of the synthesized film is generally larger than that of exfoliated MoS_2. For example, the Δk of the synthesized monolayer is found around 20.4 cm^{-1}, different from that of the exfoliated monolayer, 19.4 cm^{-1}. This could be related with certain crystalline imperfection, for example, smaller crystalline grains in the synthesized thin film. Other groups also observed a larger Δk in synthesized MoS_2 materials than exfoliated counterparts[26].

The synthesized MoS_2 thin films show unprecedented uniformity. We can find the as-grown MoS_2 thin films continuous and uniform cross an area of centimeters under optical microscope or by eyes, as illustrated by Fig. 1a and 2a. To more quantitatively assess the uniformity over a large area, we divided the monolayer MoS_2 film grown on a typical sapphire substrate in size of 1 cm × 3 cm into eight areas (Fig. 2b inset). We measured numerous Raman spectra at each of the areas, and plotted the representative results in Fig. 2b. We can find that the peak positions of the E^1_{2g} and A_{1g} modes remain identical in all the spectra. The profile of the Raman peaks, such as the FWHM, shows negligible difference. This indicates that the synthesized thin film is indeed a homogeneous monolayer with similar crystalline quality across the entire substrate. We also performed Raman mapping over an area of 10 µm × 10 µm in the as-grown monolayer film, and plotted the measured frequency difference Δk in a 2D image (Fig. 2c). All the Δk are found in a range of 20.3 – 20.7 cm^{-1}, confirming the film a homogeneous monolayer. To further confirm the uniformity, we performed multiple AFM measurements at different areas on the film, and found similar thickness and surface topology in all the AFM images (Fig. S8). A typical AFM measurement (5 µm × 5 µm) is given in Fig. 2d. It shows a continuous and smooth surface (roughness < 0.2 nm) with no step and void observed. Similar uniformity can also be found at the synthesized bilayer MoS_2 film (Fig. S9–S10). We should note that the size of the synthesized thin film (1 cm × 3 cm) is limited by the size and temperature uniformity of our current synthetic setup. We believe that by optimizing the synthetic setup we can produce wafer-scale MoS_2 monolayer or few-layer films.

The synthesized MoS_2 films exhibit a very good crystalline quality as indicted by the Raman measurements (Fig. 1e and 2b). To further elucidate the crystalline structure, we characterized the thin film using aberration-corrected scanning transmission electron microscope (STEM). To do that, we transferred the synthesized film to TEM grids following a process reported in references[25]. The synthesized film is found as polycrystalline with crystalline grains varying from tens to hundreds of nanometers as indicated by selected area electron diffraction patterns (Fig. S11). We used high angle annular dark field (HAADF) imaging to investigate the atomic arrangement in the synthesized MoS_2 monolayer and bilayer films. The monolayer and the bilayer can be identified from the folding edge of the transferred thin film (Fig. 3a inset). Fig. 3a shows typical STEM high angle

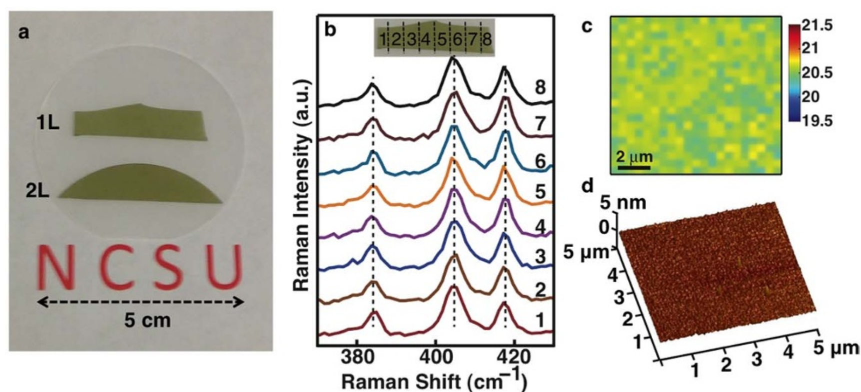

Figure 2 | Large-area uniformity of the synthesized MoS_2 monolayer and bilayer films. (a), A picture for as-grown MoS_2 monolayer (1 L) and bilayer (2 L) films, along with a NCSU logo. Underneath the films is a blank sapphire wafer, which is transparent and used as a refence. (b), Raman spectra collected from eight different areas of the MoS_2 monolayer film. The inset schematically illustrates how the eight areas distribute across the substrate. (c), Map of the Raman frequency difference Δk collected from an area of 10 μm × 10 μm in the MoS_2 monolayer film. All the measured Δk are in the range of 20.3 – 20.7 cm^{-1}. Mapping step: 0.5 μm. (d), Perspective view of a typical AFM image collected from the MoS_2 monolayer film. A topview of this AFM image is given as Fig. S7 in the Supplementary Information.

annular dark field (HAADF) image of synthesized monolayers and corresponding fast Fourier transformation (FFT) pattern. The hexagonal atomic arrangement shown in the STEM image and the FFT pattern indicate that the basal plane of the synthesized thin film is (001), i.e. the c-axis of MoS_2 materials perpendicular to the thin film. From the STEM image we can directly measure the lattice constant as $a = b = 0.32$ nm, consistent with bulk MoS_2 materials. As STEM-HAADF imaging is dependent on the atomic number, we can identify the positions of Mo and S atoms in the monolayer by the difference in image contrast (Mo atoms show much higher contrast than S atoms), as shown in Fig. 3b. Additionally, STEM-HAADF imaging provides a credible way to identify the stacking sequence in MoS_2 bilayers. We can find a substantial difference between the images of MoS_2 monolayer (Fig. 3b) and bilayer (Fig. 3c). This difference indicates an AB stacking sequence in the MoS_2 bilayer, where the Mo atoms of one layer overlap with the position of the sulfur atoms in the other layer (Fig. S13). The experimental observation matches the modeled image for the AB stacking very well (Fig. 3c).

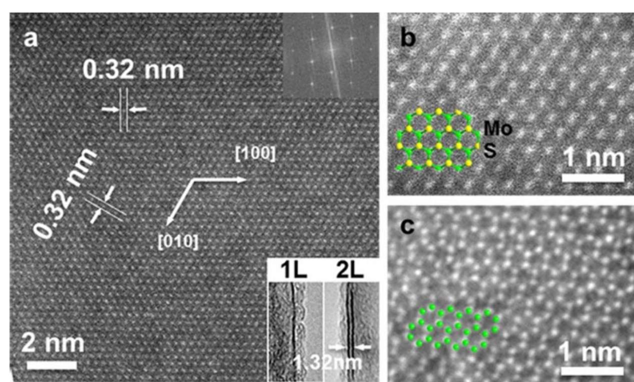

Figure 3 | Characterization of the crystal structure of synthesized MoS_2 monolayer and bilayer films. (a), High angle annular dark field (HAADF) image of typical MoS_2 monolayer film. Upper inset is the corresponding FFT pattern, which is not indexed for visual convenience (an indexed version is given in Fig. S12a). Lower inset shows the folded edges of MoS_2 monolayer and bilayer films. The lattice constant and important crystalline directions are given as shown. (b) and (c), HAADF of MoS_2 monolayer and bilayer films. The image of the bilayer film (c) is filtered and the original version is given in Fig. S12b. The insets show modeled crystal structures of MoS_2 monolayer and bilayer films with blue and yellow dots corresponding to Mo and S atoms, respectively. The sulfur atom in the inset of (c) is not given for visual convenience.

The synthesized thin films show excellent optical quality that is comparable to exfoliated MoS_2. Fig. 4a shows the PL spectra collected from exfoliated and synthesized MoS_2 monolayers. Raman peaks of the MoS_2 materials are also included, and the (photoluminescence) PL spectra are normalized to the intensity of corresponding Raman peaks. The normalization is to better correlate the measured PL intensity with the intrinsic luminescence efficiency of the materials[6]. Two peaks can be found in the PL spectra, ~ 620 nm and ~ 670 nm, and can be correlated to the B_1 and A_1 excitons of MoS_2, respectively[6]. We can find similar PL peaks from both synthesized and exfoliated MoS_2 monolayer. This suggests a comparable optical quality in the synthesized film with the exfoliated MoS_2. We should note that the synthesized monolayer for the PL measurement was grown on sapphire substrates. For the convenience of comparison with the exfoliated MoS_2, which were dispersed onto SiO2/Si substrates, the synthesized monolayer was transferred to SiO_2/Si substrates for the PL measurement (see the effect of substrates on PL in Fig. S14). We find that the PL from the MoS_2 monolayer film grown on SiO_2/Si substrates is much weaker than the films grown on sapphire (Fig. S15), probably due to a poorer crystalline quality in the films grown on SiO_2/Si substrates than those grown on sapphire as reported previously[25]. Additionally, the PL efficiency of exfoliated MoS_2 has been well known substantially decreasing with the increase in the layer number due to an evolution of the bandgap with the layer number. We can find that the PL efficiency of the synthesized MoS_2 bilayer is indeed substantially smaller than that of synthesized monolayers (Fig. S16). This suggests that the bandgap of the synthesized MoS_2 film bears a similar dependence on the layer number as exfoliated MoS_2. To illustrate the uniformity of the optical quality, we performed PL mapping over an area of 20 μm × 20 μm in the synthesized monolayer. The measurement demonstrates a uniform distribution in the PL intensity (Fig. 4a inset), confirming the uniformity as suggested by the Raman measurements shown in the preceding text.

We also evaluated the electrical quality of the synthesized MoS_2 monolayer film. We transferred the thin film grown on sapphire to degenerately doped silicon substrates covered with 280-nm-thick SiO_2, and fabricated bottom-gate transistors by evaporating 5 nm Ti/200 nm Au electrodes on top of the MoS_2 thin film. We performed electrical measurements at room temperature and in ambient environment using the degenerately doped silicon substrate as a back gate and deposited Au electrodes as the source and drain. Fig. 4b

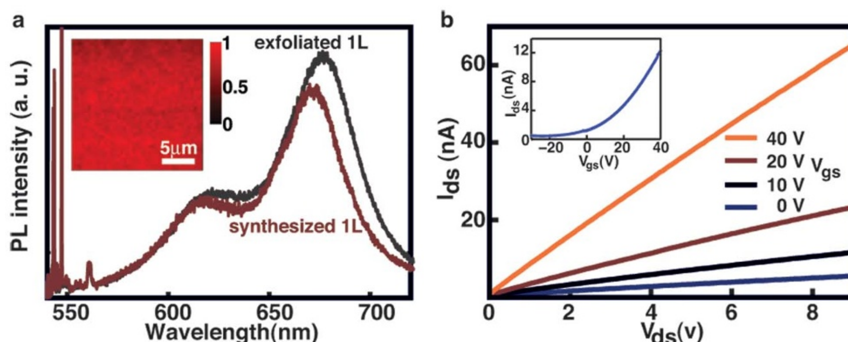

Figure 4 | Optical and electrical characterizations of the synthesized MoS_2 monolayer films. (a), Photoluminescence (PL) of the synthesized and exfoliated MoS_2 monolayers. Both were dispersed on SiO_2/Si substrates. The synthesized monolayer was grown on sapphire substrates and then transferred to SiO_2/Si substrates for the PL measurement. Using the sample substrate for the PL measurement is for the convenience of comparison. Our experimental results show the PL of MoS_2 films may be affected by the substrate (Fig. S14) (b), I_{ds}-V_{ds} curve for a field effect transistor (FET) made with the synthesized MoS_2 monolayer with gating voltages V_{gs} 0, 10, 20, 40 V. Inset, transfer characteristic for the FET with a source drain bias V_{ds} of 2 V.

shows typical output characteristic and transfer characteristic (inset) curves of the device. These results indicate that the device is an n-type channel field effect transistor, consistent with other works on exfoliated MoS_2[7,35,36]. The linear dependence of the current I_{ds} on the source-drain bias V_{ds} suggests that the contacts between the MoS_2 thin film and the electrodes are ohmic. This ensures that the observed field effect behavior is from the monolayer MoS_2 channel rather than Schottky barriers at the contact. From the measurements, we can derive the field-effect mobility of charge carriers in the device as 0.003–0.03 cm^2/V.s by using the expression $\mu = [dI_{ds}/dV_g] \times [L/(WC_iV_{ds})]$, where L and W is the length and width of the channel, respectively, C_i is the capacitance of the gating oxide, and V_g is the bias applied to the back gate. This is reasonably comparable to previous reports on exfoliated monolayers measured in similar conditions (ambient environment, back gating with silicon oxide as the gate oxide)[7,35,36]. We can thus conclude that the synthesized thin film has a reasonably comparable electrical quality with exfoliated MoS_2.

Discussion

The observed remarkable uniformity and controllability in the synthesized MoS_2 film strongly suggests that this synthetic process is self-limiting, i.e. the growth may be automatically stopped by some intrinsic factors of the synthetic process. Unlike the self-limiting mechanism for the growth of graphene[37], which is related with the limited solubility of carbon source in the catalyst of copper, our experimental results suggest that the partial pressure of gaseous MoS_2 species and the interaction of MoS_2 thin films with substrates play key roles in this self-limiting mechanism.

We found in experiments that the layer number of MoS_2 thin films increases with the amount of precursor materials (Table S1, Fig. S17–S18) and the total pressure in the synthetic setup (Fig. S19–S20). We can correlate this to the effect of the two parameters on the partial pressure of gaseous MoS_2 species P_{Mo}, which we find increasing with the amount of precursor materials and the total pressure (details see Supplementary Information). We believe that the partial pressure P_{Mo} plays an important role in control of the layer number.

To elucidate the role of P_{Mo}, we examine the dynamics of the synthetic process, and find that the precipitation reaction $MoS_2(g) \rightarrow MoS_2(s)$ is the rate-determining step, where g and s refer to gaseous and solid phases, respectively (details see Supplementary Information). The precipitation reaction is governed by two pressures, the partial pressure of gaseous MoS_2 species (P_{Mo}) and the equilibrium vapor pressure (referred as vapor pressure) of MoS_2 in solid phase (P^o_{Mo}). The role of P_{Mo} in control of the layer number is essentially rooted in its role in the thermodynamics and kinetics of the precipitation reaction. The difference between the partial pressure P_{Mo} and the vapor pressure P^o_{Mo} provides the thermodynamic driving force for the precipitation reaction. The partial pressure must be larger than the vapor pressure, i.e., $P_{Mo} > P^o_{Mo}$, to drive the precipitation of gaseous MoS_2 species. Additionally, based on the law of mass reaction, we know that the partial pressure P_{Mo} also dictates the rate of the precipitation, a larger P_{Mo} driving a faster precipitation.

The observed dependence of the layer number of MoS_2 films on experimental parameters (the amount of precursor materials and the total pressure) suggests that a larger partial pressure P_{Mo} tends to give rise to a thicker film (Fig. S21–S22). While a larger P_{Mo} can cause a larger precipitation rate, we do not think that this kinetic effect would be the major reason for the observed control of layer number. Should the precipitation rate be the major mechanism for the control, it would request a perfect control in timing to stop the precipitation right at the end of the formation of each individual layer, in order to produce the observed uniform MoS_2 films with precisely controlled layer number. This is most unlikely in our synthetic setup. The growth of large-area, highly uniform MoS_2 thin films in our experiments suggests that this precipitation is a self-limiting process, i.e. the precipitation automatically stops at the end of the formation of each individual layer.

We believe that the self-limiting mechanism may lie in a thermodynamic balance between the partial pressure of gaseous MoS_2 species (P_{Mo}) and the vapor pressure of MoS_2 thin films (P^o_{Mo}) on the substrate. The vapor pressure of MoS_2 thin films could depend on, more specifically, increase with the layer number. As P_{Mo} is requested larger than P^o_{Mo} to provide the thermodynamic driving force, the precipitation of gaseous MoS_2 species may be automatically stopped at a specific layer number by control of P_{Mo}. For instance, an exclusive growth of MoS_2 monolayer could be achieved by controlling the partial pressure P_{Mo} between the vapor pressures of MoS_2 monolayer ($P^o_{Mo,1}$) and bilayer ($P^o_{Mo,2}$) films as $P^o_{Mo,1} < P_{Mo} < P^o_{Mo,2}$. In this case, the larger vapor pressure of MoS_2 bilayers may automatically prevent the continuous growth once a MoS_2 monolayer film is formed, regardless a continuous supply of MoS_2 species. This indeed matches our observations that the lay number of MoS_2 films shows a step-function dependence on the amount of precursor materials (Table S1). Our hypothesis on the self-liming mechanism can also be supported by the observed dependence of the layer number on growth temperatures. We find that the layer number of MoS_2 film increases with the temperature of receiving substrates decreasing (Fig. S23). This can be understood that the vapor pressure of MoS_2 thin films P^o_{Mo} decreases with the temperature, and the same partial pressure P_{Mo} can drive a deposition of thicker films at lower temperatures.

The dependence of the vapor pressure of MoS_2 thin films on the layer number might be related with the interaction with substrates.

The vapor pressure indicates a capability of atoms escaping from solid phase into gas phase. The interaction of MoS_2 overlayers with substrates could substantially suppress the escaping of MoS_2 atoms, and subsequently cause a decrease in the vapor pressure. This interaction with substrates is expected to relax with the layer number (Fig. S24). As a result, the vapor pressure of MoS_2 thin film may increase with the layer number. Similar suppression effects of substrates on the vapor pressure have been well demonstrated in other materials adsorbed on substrates, for instance, polymers[38]. This dependence of vapor pressures on the layer number of MoS_2 films may provide the possibility of self-limiting growth. We also find in experiments that a precise control of the layer number generally tends to be more difficult for thicker films, for instance, larger than 4, often resulting a mixture of layer numbers. This suggests that the difference between the vapor pressures of MoS_2 films with neighboring layer number ($P^{o}_{Mo,n+1}$ - $P^{o}_{Mo,n,}$ n refers to the layer number) tends to shrink with an increase in the layer number, which makes the selective growth more difficult.

To further examine the role of the interaction with substrates, we studied the growth on different receiving substrates, the traditional three-dimensional (3D) bonded materials such as sapphire (referred as 3D substrates) and highly ordered pyrolytic graphite (HOPG, from Ted Pella) that has a similar layered structure as MoS_2 (referred as 2D substrates). We grew MoS_2 films on these different substrates under identical experimental conditions (the different substrates were placed side by side in the tube furnace). We can find a substantial difference between the films grown on sapphire and HOPG (Fig. S25). With the same experimental conditions, while the film grown on sapphire substrates is monolayer (Δk 20.4 cm^{-1}), the one grown on HOPG is bilayer (Δk 22.4 cm^{-1}). We can exclude out the possibility that the observed difference in the Raman shifts is caused by the difference in substrates (see Supplementary Information). This result confirms that the interaction of MoS_2 films with substrates plays an important role in the self-limiting growth. The strength of the interaction of 2D material overlayer with conventional 3D substrates e.g. sapphire, is well known different from that with 2D substrates (such as HOPG). This difference has been extensively manifested by the van del Waals epitaxial growth of layered materials on 2D substrates[39]. In our experiment, the different interactions of MoS_2 films with sapphire and HOPG might cause different vapor pressures. Therefore, the same partial pressure of MoS_2 can give rise to a growth of thicker MoS_2 film on HOPG.

In conclusion, we demonstrate a new chemical vapor deposition (CVD) approach that can provide capabilities to produce large-area, high quality MoS_2 monolayer and few-layer films with unprecedented uniformity and controllability. While more studies would be necessary to better understand the growth mechanism, our experimental results strongly suggest that this synthetic process is self-limiting dictated by the balance between the equilibrium pressure of MoS_2 thin films and the partial pressure of MoS_2 species in the vapor phase. As a final note, this synthetic approach can be readily scaled up to produce wafer-scale 2D MoS_2 for the development of practical electronic and photonic devices. It is poised to enable 2D MoS_2 as a useful functional material to revolutionize a wide range of fields including information technology, optoelectronics, chemical/biological sensing, and spintronics.

Methods

MoS_2 thin films were synthesized in a tube furnace as illustrated in Fig. S1. In a typical growth, 1–50 mg of molybdenum chloride ($MoCl_5$) powder (99.99%, Sigma-Aldrich) was placed at the center of the furnace and 1 g of sulfur powder (Sigma-Aldrich) were placed at the upstream entry of the furnace. Receiving substrates were placed downstream in a distance of 1–7 centimeters away from the center of the furnace. In typical experiments, the furnace was heated up at a rate of 28°C/min under a flow of Ar gas, held at a setting temperature for 10 min, and then naturally cooled down to room temperature. Typical conditions for high-quality MoS_2 thin film growth include a temperature of 850°C (the temperature for sulfur source is estimated ~ 300°C), a flow rate of 50 sccm, and a pressure around 2 Torr. The layer number of the synthetic MoS_2 thin film can be controlled by control of the amount of $MoCl_5$ precursor or the total pressure in the synthetic setup (see Supplementary Information).

The crystal structure of the resulting products were analyzed with transmission electron microscope (TEM, JEOL-2010) and probe aberration-corrected scanning transmission electron microscope (STEM, FEI Titan 80–300 STEM) operated as 200 KV under STEM mode. The as-grown thin film was transferred to TEM grid for the structure characterization. The thickness and surface topology were measured using atomic force microscope (AFM, Veeco Dimension-3000). Raman mapping and photoluminescence (PL) measurements were carried out using Horiba Labram HR800 Raman Microscopy with an excitation wavelength of 532 nm. X-ray photoelectron spectroscopy were performed on SPECS XPS using an Mg Kα x ray source. The field-effect transistor device was fabricated by evaporating Ti/Au (5/200 nm) electrodes directly onto top of MoS_2 films transferred to degenerately doped Si substrates with 280 nm thick silicon oxide. A copper grid (100mesh, 30 micron spacing, Ted Pella) was placed on top of the thin film as mask for the electrode fabrication. This gives a relative large channel with a length L = 30 μm and a width W = 230 μm. The electrical measurements were performed in ambient conditions using a probe station (Karl Suss PSM6).

1. Novoselov, K. S. *et al.* Two-dimensional Gas of Massless Dirac Fermions in Graphene. *Nature* **438**, 197–200 (2005).
2. Berger, C. *et al.* Electronic Confinement and Coherence in Patterned Epitaxial Graphene. *Science* **312**, 1191–1196 (2006).
3. Huang, X., Qi, X. Y., Boey, F. & Zhang, H. Graphene-Based Composites. *Chem. Soc. Rev.* **41**, 666–686 (2012).
4. Huang, X. *et al.* Graphene-Based Materials: Synthesis, Characterization, Properties, and Applications. *Small* **7**, 1876–1902 (2011).
5. Mak, K. F., Lee, C., Hone, J., Shan, J. & Heinz, T. F. Atomically Thin MoS2: A New Direct-Gap Semiconductor. *Phys. Rev. Lett.* **105**, 136805 (2010).
6. Splendiani, A. *et al.* Emerging Photoluminescence in Monolayer MoS2. *Nano Lett.* **10**, 1271–1275 (2010).
7. Radisavljevic, B., Radenovic, A., Brivio, J., Giacometti, V. & Kis, A. Single-layer MoS2 Transistors. *Nat Nanotechnol* **6**, 147–150 (2011).
8. Wang, H. *et al.* Integrated Circuits Based on Bilayer MoS2 Transistors. *Nano Lett.* **12**, 4674–4680 (2012).
9. Yin, Z. Y. *et al.* Single-Layer MoS2 Phototransistors. *ACS Nano* **6**, 74–80 (2012).
10. Pu, J. *et al.* Highly Flexible MoS2 Thin-Film Transistors with Ion Gel Dielectrics. *Nano Lett.* **12**, 4013–4017 (2012).
11. Kim, S. *et al.* High-mobility and Low-power Thin-film Transistors Based on Multilayer MoS2 Crystals. *Nat. Comm.* **3**, 1011 (2012).
12. Yoon, Y., Ganapathi, K. & Salahuddin, S. How Good Can Monolayer MoS2 Transistors Be? *Nano Lett.* **11**, 3768–3773 (2011).
13. Cao, T. *et al.* Valley-selective Circular Dichroism of Monolayer Molybdenum Disulphide. *Nat. Comm.* **3**, 887 (2012).
14. Gunawan, O. *et al.* Valley Susceptibility of an Interacting Two-dimensional Electron System. *Phys. Rev. Lett.* **97**, 186404 (2006).
15. Lee, H. S. *et al.* MoS2 Nanosheet Phototransistors with Thickness-Modulated Optical Energy Gap. *Nano Lett* **12**, 3695–3700 (2012).
16. Mak, K. F. *et al.* Tightly Bound Trions in Monolayer MoS2. *Nat. Mater.* **12**, 207–211 (2012).
17. Mak, K. F., He, K., Shan, J. & Heinz, T. F. Control of Valley Polarization in Monolayer MoS2 by Optical Helicity. *Nat. Nanotechnol.* **7**, 494–498 (2012).
18. Xiao, D., Liu, G. B., Feng, W. X., Xu, X. D. & Yao, W. Coupled Spin and Valley Physics in Monolayers of MoS2 and Other Group-VI Dichalcogenides. *Phys. Rev. Lett.* **108**, 196802 (2012).
19. Zeng, H., Dai, J., Yao, W., Xiao, D. & Cui, X. Valley Polarization in MoS2 Monolayers by Optical Pumping. *Nat. Nanotechnol.* **7**, 490–493 (2012).
20. Chhowalla, M. *et al.* The Chemistry of Ultra-thin Transition Metal Dichalcogenide Nanosheets. *Nat. Chem.* **5** (2013).
21. He, Q. *et al.* Fabrication of Flexible MoS2 Thin-Film Transistor Arrays for Practical Gas-Sensing Applications. *Small* **8**, 2994–2999 (2012).
22. Huang, X., Zeng, Z. & Zhang, H. Metal Dichalcogenide Nanosheets: Preparation, Properties and Applications. *Chem. Soc. Rev.* **42**, 1934–1946 (2013).
23. Liu, J. *et al.* Preparation of MoS2-Polyvinylpyrrolidone Nanocomposites for Flexible Nonvolatile Rewritable Memory Devices with Reduced Graphene Oxide Electrodes. *Small* **8**, 3517–3522 (2012).
24. Lee, Y.-H. *et al.* Synthesis of Large-Area MoS2 Atomic Layers with Chemical Vapor Deposition. *Adv. Mater.* **24**, 2320–2325 (2012).
25. Etgar, L. *et al.* High Efficiency Quantum Dot Heterojunction Solar Cell Using Anatase (001) TiO2 Nanosheets. *Adv. Mater.* **24**, 2202–2206 (2012).
26. Zhan, Y., Liu, Z., Najmaei, S., Ajayan, P. M. & J, L. Large-Area Vapor-Phase Growth and Characterization of MoS2 Atomic Layers on a SiO2 Substrate. *Small* **8**, 966–971 (2012).
27. Lin, Y. C. *et al.* Wafer-scale MoS2 Thin Layers Prepared by MoO3 Sulfurization. *Nanoscale* **4**, 6637–6641 (2012).
28. Zhang, W. *et al.* Ultrahigh-Gain Phototransistors Based on Graphene-MoS2 Heterostructures. *arXiv:1302.1230* (2013).
29. Shi, Y. *et al.* van der Waals Epitaxy of MoS2 Layers Using Graphene As Growth Templates. *Nano Lett.* **12**, 2784–2791 (2012).
30. Najmaei, S. *et al.* Vapor Phase Growth and Grain Boundary Structure of Molybdenum Disulfide Atomic Layers. *arXiv 1301.2812* (2013).

31. Zande, A. M. v. d. *et al*. Grains and Grain Boundaries in Highly Crystalline Monolayer Molybdenum Disulfide. *arXiv 1301.1985* (2013).
32. Lee, C. *et al*. Anomalous Lattice Vibrations of Single- and Few-Layer MoS2. *ACS Nano* **4**, 2695–2700 (2010).
33. Li, H. *et al*. From Bulk to Monolayer MoS2: Evolution of Raman Scattering. *Adv. Func. Mater.s* **22**, 1385–1390 (2012).
34. Li, S.-L. *et al*. Quantitative Raman Spectrum and Reliable Thickness Identification for Atomic Layers on Insulating Substrates. *ACS Nano* **6**, 7381–7388 (2012).
35. Novoselov, K. S. *et al*. Two-dimensional Atomic Crystals. *Proc. Natl. Acad. Sci. USA* **102**, 10451–10453 (2005).
36. Li, H. *et al*. Fabrication of Single- and Multilayer MoS2 Film-Based Field-Effect Transistors for Sensing NO at Room Temperature. *Small* **8**, 63–67 (2012).
37. Li, X. *et al*. Large-Area Synthesis of High-Quality and Uniform Graphene Films on Copper Foils. *Science* **324**, 1312–1314 (2009).
38. Podgornik, P. & Parsegian, V. A. On a Possible Microscopic Mechansm Underlying the Vapor Pressure Paradox. *Biophys. J.* **72**, 942–952 (1997).
39. Ueno, K., Saiki, K., Shimada, T. & Koma, A. Epitaxial Growth of Transition Metal Dichalcogenides on Cleaved Faces of Mica. *J. Vac. Sci. Technol. A* **8**, 68 (1990).

Acknowledgments

The authors would like to thank Yuntian Zhu for providing access to a Raman spectrometer. L. C. acknowledges a Ralph E. Powe Junior Faculty Enhancement Award for Oak Ridge Associated Universities. Y. Z. acknowledges the support of Bissell Distinguished Professorship. Part of the work was supported by the Army Research Office (W911NF-11-1-0529).

Author contributions

Y.Y. and L.C. conceived the experiments. Y.Y. and C.L. perfermed the synthesis. Y.Y. performed most of the characterizations and device fabrications. Y.L. carried out the STEM characterization. L.S and Y.Z. performed the Raman and PL mapping. Y.Y. and L.C. analyzed the data. All authors were involved in writing the manuscript.

Additional information

Supplementary information accompanies this paper at http://www.nature.com/scientificreports

Competing financial interests: The authors declare no competing financial interests.

License: This work is licensed under a Creative Commons Attribution-NonCommercial-NoDerivs 3.0 Unported License. To view a copy of this license, visit http://creativecommons.org/licenses/by-nc-nd/3.0/

How to cite this article: Yu, Y. *et al*. Controlled Scalable Synthesis of Uniform, High-Quality Monolayer and Few-layer MoS_2 Films. *Sci. Rep.* **3**, 1866; DOI:10.1038/srep01866 (2013).